POLITECNICO DI TORINO
Repository ISTITUZIONALE

Masonry arches and vaults under fire

Original
Masonry arches and vaults under fire / Fantilli, A.P., Burello, N.S.. - In: JOURNAL OF BUILDING ENGINEERING. - ISSN 2352-7102. - 56:104740(2022). [10.1016/j.jobe.2022.104740]

Availability:
This version is available at: 11583/2979458 since: 2023-06-21T11:36:05Z

Publisher:
Elsevier

Published
DOI:10.1016/j.jobe.2022.104740

Terms of use:

This article is made available under terms and conditions as specified in the corresponding bibliographic description in the repository

Publisher copyright

(Article begins on next page)

30 June 2026

Journal of Building Engineering 56 (2022) 104740

Contents lists available at ScienceDirect

Journal of Building Engineering

journal homepage: www.elsevier.com/locate/jobe

Masonry arches and vaults under fire

Alessandro P. Fantilli *, Nicholas S. Burello

Politecnico di Torino - DISEG, Corso Duca degli Abruzzi 24, 10129, Torino, Italy

ARTICLE INFO

Keywords:
Curvilinear structures
Structural design
Limit analysis
Reduced cross-section
Standard fire

ABSTRACT

Arches and vaults subjected to elevated temperatures are herein investigated. For these elements, widely present in historical buildings, structural models under fire scenario are still undefined, also due to the lack of full-scale tests. Indeed, the simplified procedure generally used to assess the capacity of walls and columns (as reported in the annex C of Eurocode 6 part 1–2) needs to be extended to masonry curvilinear structures. Accordingly, with the aim of predicting the load-bearing capacity of arches and vaults, limit analysis is applied to reduced cross-sections. To validate this approach, new laboratory tests were also carried out on barrel vaults subjected to the standard fire in the intrados, and different distributed loads on the extrados. Similarly to the application of simplified models, a conservative estimation of the fire resistance is generally provided by the proposed approach.

1. Introduction

In the past, arches and vaults were used to build horizontal structural members with materials having a negligible tensile strength (e.g., stone units or clay bricks and lime mortar). Although nowadays they have been substituted by steel and reinforced concrete, curvilinear masonry structures are still widely present in existing bridges [1] and buildings [2].

To assess the capacity of masonry structures, two approaches can be adopted [3]: incremental-iterative analysis [4] and limit analysis [5,6]. Both of them can be carried out in compliance with code rules (e.g., Eurocode 6, part 1-1 [7]), when masonry structures are subjected to ordinary loads [8–11]. Nevertheless, exceptional loads, such as those produced by fire exposure, must be considered in several circumstances. In other words, design purposes often require the fire resistance R (expressed in minutes) of structures subjected to the standard fire [12].

Due to a large number of tests on walls and columns under fire [13–15], R can be evaluated by applying either tabulated data [16] or calculation methods (both simplified [17] and advanced [18–20]). The results provided by theoretical models are in good agreement with those experimentally measured when material properties (i.e., compressive strength, tensile strength, thermal expansion, etc.) are defined as a function of the temperature [21–26].

Only when the results of fire tests performed on arches and vaults are available, could the approaches used for linear vertical elements be extended to the horizontal and curvilinear structures. Unfortunately, this is not possible because experimental data and theoretical analysis are rather demanding [27], to such an extent that Eurocode 6 part 1–2 [16] cannot be applied to arches and vaults. Indeed, an advanced search on Scopus database (keywords: “Masonry materials” and “Arches” and “Fire resistance”) leads to the conclusions that neither experimental data nor numerical models are present in the current literature. To the author’s knowledge, only a report of the Italian fire department [28] is available. More precisely, they tested a masonry barrel vault subjected to concentrated loads (in addition to self-weight) on the extrados and to the standard fire in the intrados.

* Corresponding author.
E-mail addresses: alessandro.fantilli@polito.it (A.P. Fantilli), nicholas.burello@polito.it (N.S. Burello).

https://doi.org/10.1016/j.jobe.2022.104740
Received 25 March 2022; Received in revised form 16 May 2022; Accepted 30 May 2022
Available online 1 June 2022
2352-7102/© 2022 The Authors. Published by Elsevier Ltd. This is an open access article under the CC BY-NC-ND license (http://creativecommons.org/licenses/by-nc-nd/4.0/).

A new numerical model, based on the limit analysis and the residual cross-section method, is herein proposed to calculate R in curvilinear masonry structures (Section 2). The goal is to extend the simplified calculation method, currently applied to walls and columns [16], to the most common geometries of vaults and arches, still widely present in existing buildings. Moreover, to enrich the database of experimental results and validate the proposed approach, new barrel vaults (subjected to different load arrangements) were tested under fire scenario. The new fire investigations are described and reported in Section 3, whereas Section 4 shows the comparison between numerical and experimental results.

1.1. Research signifiance

Masonry arches and vaults can be found in existing buildings and bridges. Most of the analyses performed on these structural elements were introduced to predict the bearing capacity in case of ordinary loads. Conversely, studies on fire resistance of masonry curvilinear structures are very scarce in the technical literatures. The authors believe that the proposed theoretical model, as well as the experimental analyses, dealing with arches and vaults subjected to elevated temperatures, are carried out for the first time and can be very useful to assess existing buildings.

2. Numerical analysis

The automatization of the limit analysis, applied to vaults and arches [5,29], is the main aspect of the proposed model. The goal is to compute the number of acceptable Line Of Thrust (LOT), taking into account the reduction of cross-sectional thickness due to fire exposure. As described in the following sections, the model consists of three stages: structural discretization, calculation of LOTs, and fire assessment.

2.1. Stage1: structural discretization

In the case of curvilinear structures with an axis of symmetry, only one of the halves can be analysed (Fig. 1). It is divided into N blocks, starting from the support ($i = 1$) up to the keystone ($i = N$). The forces (i.e., $P_{G1,i}$ = self-weight, $P_{G2,i}$ = permanent load due to the backfill material, $P_{Qv,i}$ = live loads, P_I = concentrated load applied to the I^{th} cross-section) acting on the i^{th} block ($1 \le i \le N$) are calculated with the following equations:

$$P_{G1,i} = \frac{\gamma_{G1} \cdot \Delta z \cdot \frac{H_{b,I} + H_{b,I-1}}{2} \cdot b_1}{\cos(\alpha_i)} \tag{1}$$

$$P_{G2,i} = \gamma_{G2} \cdot b_2 \cdot \Delta z \cdot \frac{\left[\left(y_{sup,I-1} - y_{I-1} - \frac{H_{b,I-1}}{2 \cdot \cos(\alpha_{i-1})}\right) + \left(y_{sup,I} - y_I - \frac{H_{b,I}}{2 \cdot \cos(\alpha_i)}\right)\right]}{2} \tag{2}$$

$$P_{Qv,i} = Q_v \cdot b_3 \cdot \Delta z \tag{3}$$

where γ_{G1} = density of the structural material; γ_{G2} = density of the backfill material; Q_v = live load; b_1 = width of the masonry cross section; b_2 = width of the backfill material; b_3 = width used to compute the live load; $H_{b,I}$ = depth of the I^{th} cross-section (I and I-1 refers to the limits of the i^{th} block); $\Delta z_i = z_I - z_{I-1}$ = length of the i^{th} block; α_i = angle of inclination of the i^{th} block; $y_{sup,I}$ = ordinate of the

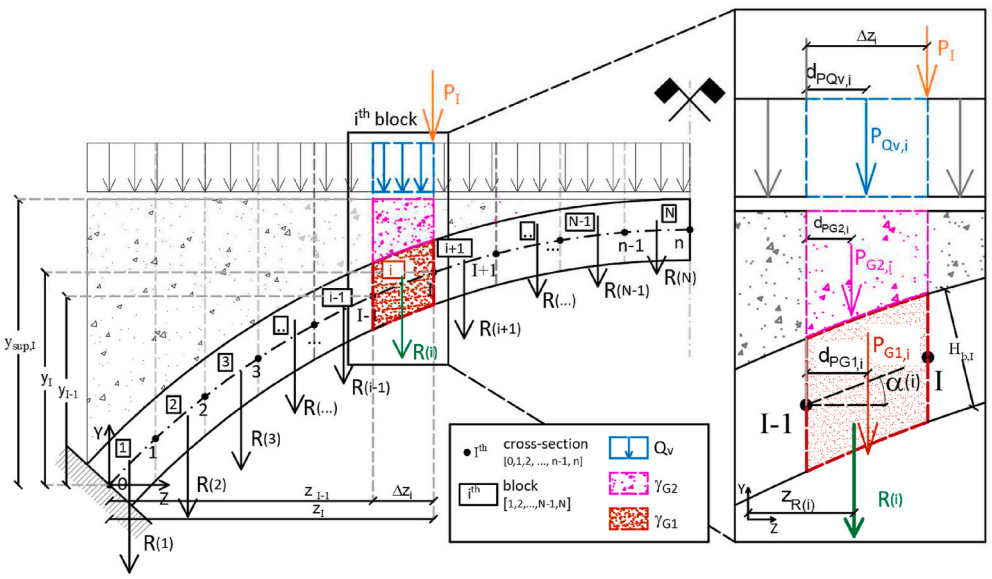

Fig. 1. Discretization of a generic curvilinear structure with an axis of symmetry.

upper edge of the backfill material in correspondence of the I^{th} cross-section.

The resultant of the vertical loads R_{TOT}, and its distance z_{Rtot} from the origin (of [YZ] axes), are calculated as:

$$R_{tot} = \sum_{i=1}^{N} R(i) = \sum_{i=1}^{N} P_{G1,i} + P_{G2,i} + P_{Qv,i} + P_I \tag{4}$$

$$z_{Rtot} = \frac{\sum_{i=1}^{N} R(i) \cdot z_R(i)}{R_{tot}} = \frac{\sum_{i=1}^{N} R(i) \cdot \left[z_{i-1} + \frac{P_{G1,i} \cdot d_{PG1,i} + P_{G2,i} \cdot d_{PG2,i} + P_{Qv} \cdot d_{PQv,i} + P_I \cdot \Delta z_i}{R(i)} \right]}{R_{tot}} \tag{5}$$

where $R(i)$ = resultant of the i^{th} block; $z_{R(i)}$ = distance of $R(i)$ from the origin of [YZ] axes; $d_{PG1,i}$, $d_{PG2,i}$ and $d_{PQv,i}$ are, respectively, the distances of the forces $P_{G1,i}$, $P_{G2,i}$ and $P_{Qv,i}$ from the I^{th}-1 cross-section (see Fig. 1).

2.2. Stage2: calculation of the lines of thrust

Under the hypothesis that spalling does not occur, the forces previously defined remain constant during the exposure to the elevated temperatures. As illustrated in Fig. 2, the geometry of each LOT is a function of the points of passage "A"- in correspondence of the support ($I = 0$), and "B" – on the axis of symmetry ($I = n$).

A and B can assume any position within the depth of the two cross sections, moving from the intrados ($j = 0$) to the extrados ($j = m$, where m = number of points used to divide the depth $H_{b,I}$). In particular, the coordinates of these points are:

$$point\ A \begin{cases} z_k(A) = z_0 + \frac{H_{b,0}}{2} \cdot \sin\alpha_0 - \frac{H_{b,0}}{m} \cdot \sin\alpha_0 \cdot j \\ y_k(A) = y_0 - \frac{H_{b,n}}{2} \cdot \cos\alpha_0 + \frac{H_{b,n}}{m} \cdot \cos\alpha_0 \cdot j \end{cases} \quad j = 0, 1, \ldots, m \tag{6}$$

$$point\ B \begin{cases} z_k(B) = z_N \\ y_k(B) = y_N - \frac{H_{b,n}}{2} + \frac{H_{b,n}}{m} \cdot j \end{cases} \quad j = 0, 1, \ldots, m \tag{7}$$

where $1 \leq k \leq m \times m$ refers to the k^{th} LOT calculated after fixing the points A and B (see Fig. 2). For each couple of these points, the intensity of the horizontal force H_k, the angle of inclination β_k, and the reaction S_k of the support can be calculated as follows:

$$\tan(\beta_k) = \frac{z_{Rtot} - z_{k(A)}}{y_{k(B)} - y_{k(A)}} \tag{8}$$

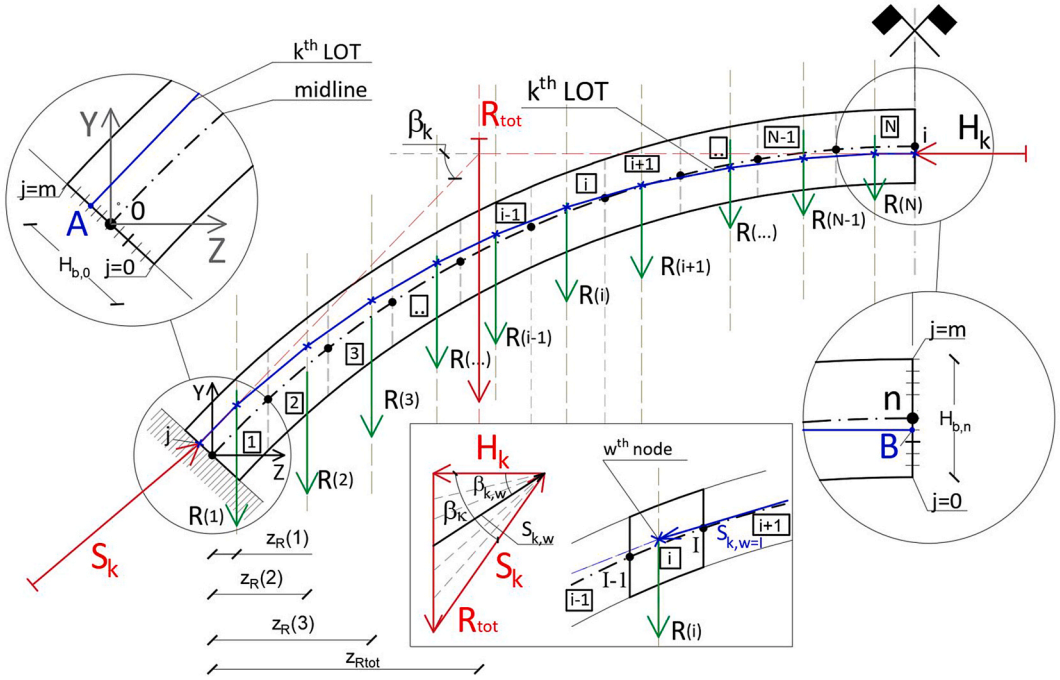

Fig. 2. Computation of the kth line of thrust (A and B are arbitrarily chosen).

$$H_k = R_{tot} \cdot \tan(\beta_k) \tag{9}$$

$$S_k = \sqrt{R_{tot}^2 + H_k^2} \tag{10}$$

Accordingly, each LOT is a polygonal line with $N+2$ points, including A, B, and the points that lie on the lines of action of $R(i)$. For the k^{th} line of thrust, the intensity of the force $S_{k,w}$, the inclination $\beta_{k,w}$ (with respect to the horizontal direction), and the coordinates of w^{th} node are:

$$S_{k,w} = \sqrt{\sum_{i=w+1}^{N} R(i)^2 + H_k^2} \tag{11}$$

$$\tan(\beta_{k,w}) = \frac{\sum_{i=w+1}^{N} R(i)}{H_k} \tag{12}$$

$$w = \begin{cases} z_k(w) = z_R(w) \\ y_k(w) = y_{w+1} - tan(\beta_{k,i}) \cdot (z_k(w+1) - z_k(w)) \end{cases} \quad if\ w = 1, \ldots, N \tag{13}$$

The calculation is repeated for each combination of A and B, obtaining $m \times m$ lines of thrust.

2.3. Stage3: fire assessment

Although the points A and B are always within the cross sections (see Fig. 2) at $I = 0$ and $I = N+1$, respectively, not all the $m \times m$ lines of thrust are acceptable. In fact, for a given fire duration, some parts of LOT may fall outside the resisting cross section. In addition, the applied actions $S_{k,w}$ can generate compressive stresses higher than the compressive strength [30].

To take into account both these situations, the thickness of the ineffective cross section can be calculated by following the reduced cross section approach, currently adopted for vertical members (see, for instance, Eurocode 6 Part 1–2 [16]). Referring to Fig. 3a, the part of the cross section having a temperature T higher than θ_2 (zone 1 in Fig. 3a) is ineffective, therefore the compressive strength of masonry is $f_{d\theta 2} = 0$. In the coldest zone (zone 3 in Fig. 3a), $T < \theta_1$ and $f_{d\theta\,1} = f_{d20}$ (f_{d20} is the compressive strength measured at 20 °C). When $\theta_1 \le T \le \theta_2$, the masonry is partially damaged, and an intermediate compressive strength (i.e., $f_{d\theta 2} = 0 \le f_d \le f_{d\theta 1} = f_{d20}$) has to

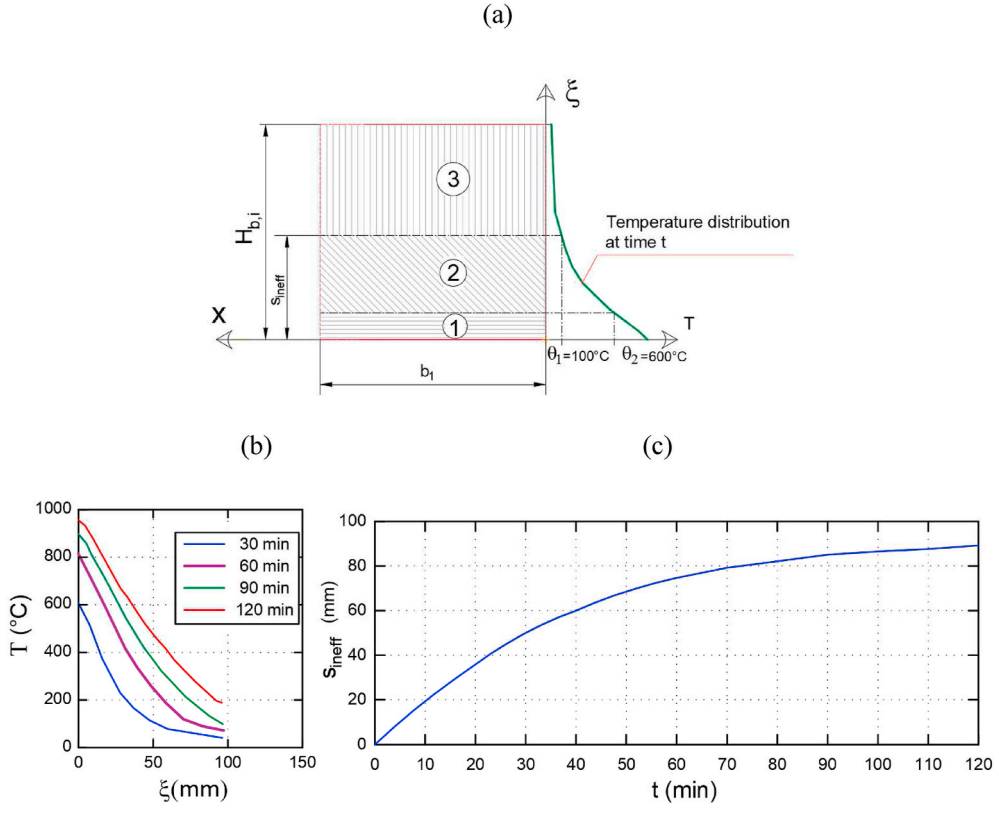

Fig. 3. Fire assessment of masonry cross-sections: (a) the resisting zones for a given temperature profile; (b) temperature distributions in the case of "clay units with general purpose mortar" (θ_1 = 100 °C, θ_2 = 600 °C [13]); (c) evolution of s_{ineff} with the time of fire exposure.

be assumed. For instance, $\theta_2 = 600$ °C and $\theta_1 = 100$ °C are suggested in the case of "Clay units with general purpose mortar" (see Fig. 3b).

In the absence of experimental data, according to some national annexes of Eurocode 6, the compressive strength can be conservatively assumed equal to zero also in the zones where $\theta_1 \leq T \leq \theta_2$. In other words, the part of the cross section at temperatures higher than θ_1 (i.e., 100 °C in Fig. 3b) is ineffective. Thus, by using the curves of Fig. 3b, the temperature distribution in each cross-section of curvilinear structures is known. However, a more rigorous calculation can be performed by means of a finite element thermal analysis [31].

As the distribution of temperatures changes with the time (Fig. 3b), the ineffective thickness s_{ineff} (of zones 1 and 2 in Fig. 3a) increases (see Fig. 3c). As a consequence, the number of LOTs which fall within the resisting zone tends to reduce. For instance, in Fig. 4a the LOTs coloured in blue are acceptable, whereas those in red fall outside the resisting thickness and cannot be accepted.

The selection of the acceptable LOT must be also based on the mechanical properties of masonry. Assuming no tensile strength and the absence of shear failure, the acceptability criterium of the blue curves must furtherly include the assessment of compressive stress $\sigma_{Ed,w}$, which should be lower than $f_d = f_{d20}$ in each node. Fig. 4b illustrates the resisting section (zone 3) in the w^{th} node of the k^{th} thrust line, where the following condition has to be satisfied:

$$\sigma_{Ed,w} = \frac{S_{k,w}}{b_1 \cdot 2 \cdot \left[\frac{\left(H_{b,I} - s_{ineff}\right)}{2} - e_{k,w} \right]} < f_d \tag{14}$$

where $e_{k,w}$ = eccentricity of the force $S_{k,w}$.

As resisting cross-section of curvilinear structures reduces with the exposure to elevated temperatures, the fire capacity R is the maximum time at which the number of acceptable LOT remains greater than zero.

3. Experimental investigations

3.1. Geometry, materials, and test setup

Each test consisted of a masonry barrel vault supported by two steel beams (HE200B), which covered the roof of a laboratory oven (see Fig. 5). A polystyrene centering (Fig. 6a) was used to layering bricks and mortar joints of the two vaults, hereinafter called vault #1 (Fig. 6b) and vault #2 (Fig. 6c), respectively.

Both the vaults had a clean span length of 2285 mm, with an intrados radius equal to 1490 mm (rise = 483 mm), a single ring cross-section of 1030 × 120 mm^2 (see Table 1), and a mean bed joint thickness of 10 mm. Among the existing masonries, it is difficult to find the most representative types of units and mortars. Thus, materials available on the current market, already used in the previous test [28], were adopted. In particular, clay bricks (55 × 120 × 250 mm^3) having a mean compressive strength $f_b = 40.8$ N/mm^2, and premixed cement-lime based mortar M5 (compressive strength $f_m > 5$ N/mm^2) were the constituent materials of the vaults. The above-mentioned values are those declared by producers.

As the masonry strength can vary depending on the arrangement of bricks and mortars, the specimens adopted in this project are similar to those used by Alecci et Al [32]. (Fig. 7a) and by VVF [28] (Fig. 7b) in previous investigations. Both the types were made of three layers of bricks and two mortar joints with a thickness of 10 mm, but having different shapes and sizes, as shown in Fig. 7. The compressive strength was measured on three samples for each type of prism at 20 °C, as reported in Table 2. The minimum compressive strength (i.e., $f_m = 14.50$ N/mm^2) is herein used for the structural analysis of the vaults under fire.

In addition to the self-weight, distributed loads were differently arranged (see Table 3). Vault #1 (Fig. 6b) was only subjected to the weight of backfill (made with loose sand of density $\gamma_s = 13.75$ kN/m^3), whereas lightweight concrete backfill (with a density $\gamma_c = 20$ kN/m^3) and distributed live load ($Q_v = 2.1$ kN/m^2) were applied on vault #2 (Fig. 6c). Gas burners generated the fire within the oven (at the intrados of each vault), and increased the environmental temperature according to the standard temperature-time curve [12]:

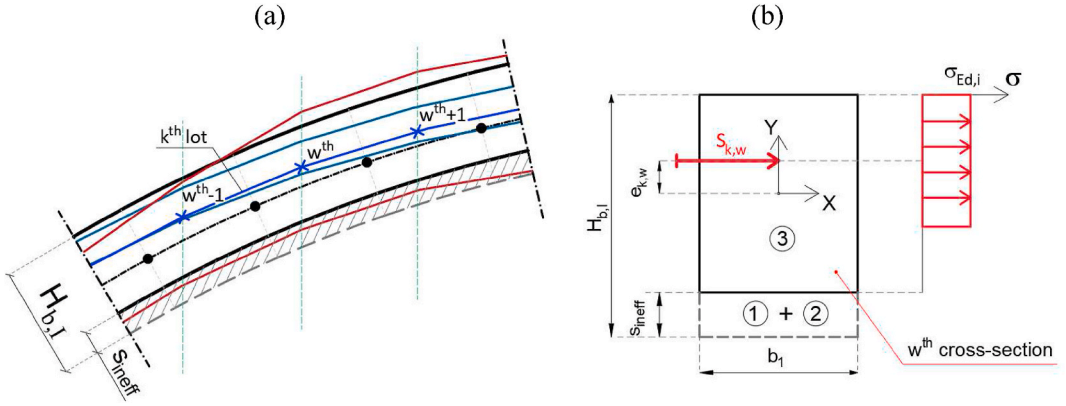

Fig. 4. Acceptable lines of thrust with respect to (a) geometrical properties of the vault and (b) with respect to the static condition in the wth node.

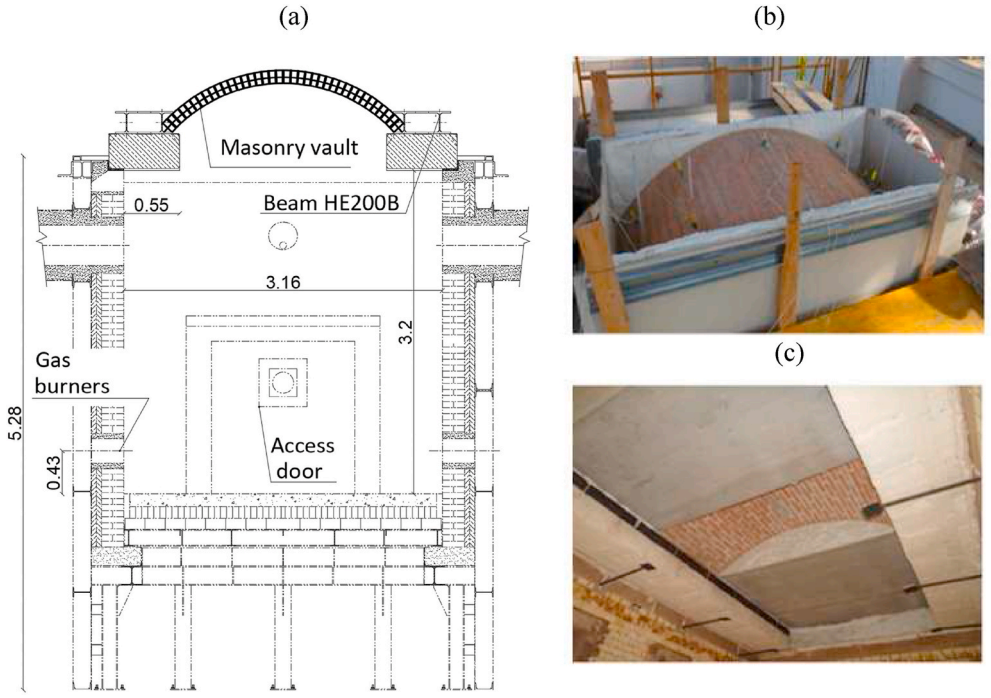

Fig. 5. Setup of fire investigations: (a) cross-section of the oven used to test the vaults; (b) external view of vault #1; (c) view of the intrados of vault #1 (lengths in m).

$$T = 20 + 345 \log(8\,t{+}1)\ [^{\circ}\mathrm{C}] \tag{15}$$

where t = time expressed in minutes.

As known, in the limit analysis of arches and vaults, the failure occurs when the four-hinge mechanism takes place. In the case of unreinforced single-ring masonry arches, several authors [32–36] observed the formation of this mechanism by measuring the deflections in some points of the structure, while external loads increased. Accordingly, a total of 6 LVDTs were placed along the extrados of the barrel vaults (2 on the arch-crown, 2 at 530 mm and 2 at 930 mm from the mid-span - see Fig. 8) to measure the displacements during the fire exposure.

3.2. Experimental results

The standard fire lasted 90 min in vault #1 and 115 min in vault #2. Both the tests were stopped in order to keep the safety conditions within the laboratory, although neither collapse nor material spalling were observed.

Fig. 9a and Fig. 9b show the displacements measured during the exposure to the standard fire in vault #1 and vault #2, respectively. Deflections are negative (raising) at the crown and positive (settlement) close to the springers. This phenomenon is ascribed to restrained thermal expansion of statically indeterminate structures, which tends to generate tensile stresses on the unexposed surface around the axis of symmetry. Thus, the vaults were affected by an evident cracking phenomenon at the crown (failure of brick-mortar interface), where the first hinge appears (see Fig. 10).

Other cracks were not observed in the vaults, both during the exposure to fire (the oven was inaccessible) and after the cooling stage, when the vertical displacements vanished, and cracks closed. Thus, the presence of other hinges can only be conjectured from the distribution of the displacements depicted in Fig. 9a and b. As the sign of the deflection changes (from raising to settlement) moving from the crown to the springers, further hinges must be localised in between. In particular, the displacements are compatible with the presence of 3 hinges (in both the vaults), whose positions are qualitatively illustrated in Fig. 11a (vault #1) and Fig. 11b (vault #2). Due to the unavoidable heterogeneity of masonry properties, hinges are asymmetrically located with respect to the keystone of vault #2. Consequently, negative displacements appeared close to the left springer during the first minutes of the fire exposure (see Fig. 9b).

Similar to unreinforced arches subjected to direct loads [32–36], it appears reasonable to assume that the failure of curvilinear structures will occur by the four-hinge mechanism also during the exposure to the standard fire. In addition, as visual inspection revealed the absence of spalling at the end of the tests, the assumption of constant loads during the fire exposure (see Section 2.1) seems to be acceptable.

4. Comparisons between prediction and experimental result

To validate the limit analysis proposed herein, the predicted loadbearing capacities are compared with those experimentally measured in some arches and vaults with and without fire.

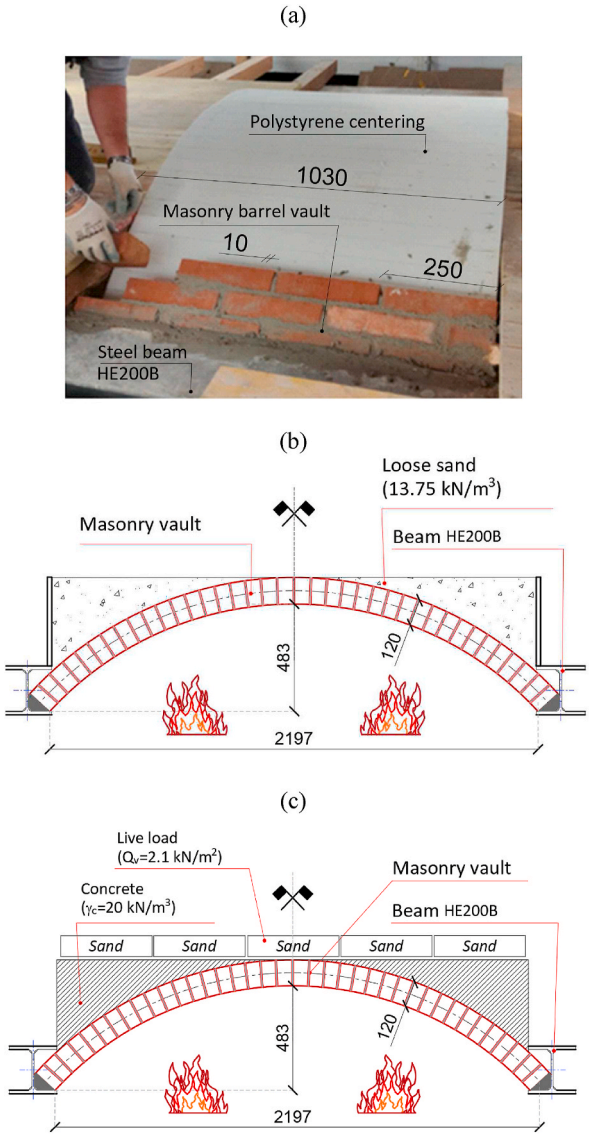

Fig. 6. The curvilinear masonry prototypes: (a) use of polystyrene centering during the construction phase; (b) geometry of vault #1; (c) geometry of vault #2 (measures in mm).

Table 1
Geometrical properties of the barrel vaults tested in this project.

Parameters		vault #1 and vault #2
Span	(mm)	2197
Rise	(mm)	483
Thickness	(mm)	120
Width	(mm)	1030
Intrados radius	(mm)	1490
Arch angle	(°)	95

4.1. An arch without fire action

Zampieri et al. [35] measured the ultimate load of the unstrengthened masonry arch depicted in Fig. 12a. Both the geometrical and material properties of the curvilinear structure are reported in Table 4. The load P, applied in the arch crown, was monotonically increased up to the failure (ultimate load $P_u = 0.44$ kN).

As the test was carried out at environmental temperature (20 °C), the proposed model is simply used to estimate P_u (i.e., $s_{ineff} = 0$

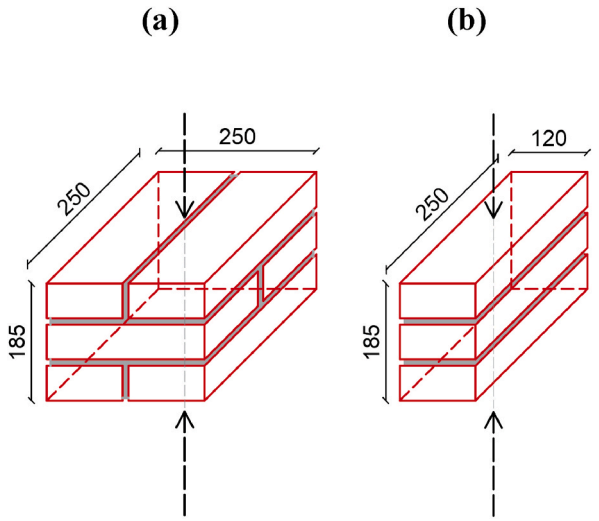

Fig. 7. Uniaxial compression tests on masonry prisms: (a) type A; (b) type B.

Table 2
Results of the uniaxial compression tests on masonry prisms. (s.d. = standard deviation; COV = coefficient of variation).

Specimen	Compressive strength (MPa)	s.d. (MPa)	COV
Type A	19.10	1.06	0.055
Type B	14.50	1.47	0.102

Table 3
Concentrated and distributed loads applied on barrel vaults tested in this project.

Parameters		vault #1	vault #2
Self-weight	(kN/m^3)	17.00	17.00
Backfill	(kN/m^3)	13.75	20.00
Live loads	(kN/m^2)	0	2.10

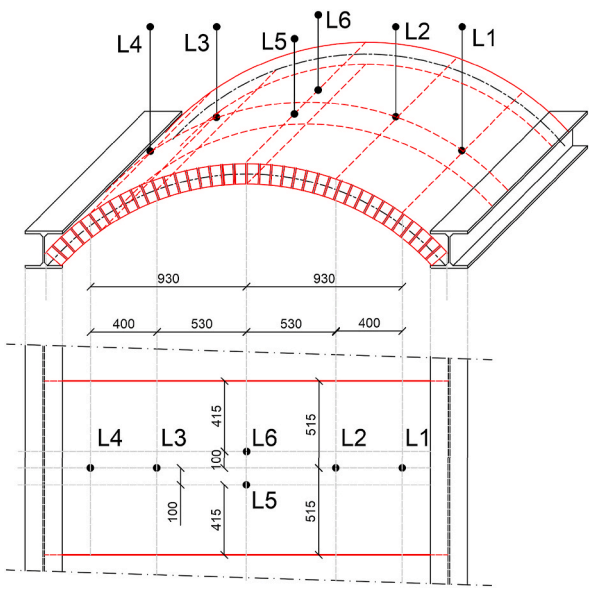

Fig. 8. Position of the LVDTs used to measure the displacements in vault #1 and vault #2 (lengths in mm).

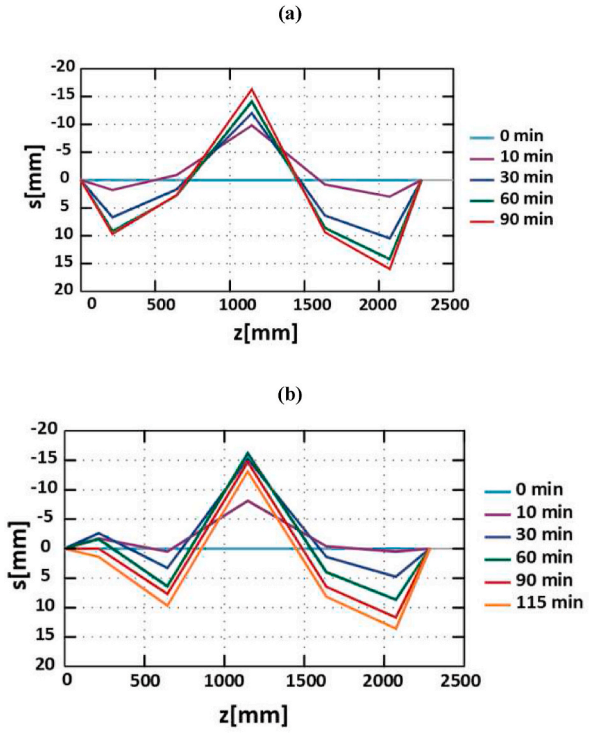

Fig. 9. Displacements measured during the fire exposure in (a) vault #1 and (b) vault #2. (where, according to the reference system shown in Fig. 1, s [mm] = vertical displacements along Y axis; and z [mm] = distance from the left end along Z axis).

Fig. 10. Failure of brick/mortar interface at arch-crown of vault #1 during the fire exposure.

mm in Fig. 3a), in correspondence of which none of the computed LOT is acceptable. However, to perform a correct limit analysis, suitable values of N (i.e., number of blocks - Fig. 1) and m (i.e., points of passage of LOT - Fig. 2) must be used, because numerical outcomes may be affected by these parameters.

Fig. 12b, where the number of acceptable LOT is plotted as a function of the applied load P, shows the variation of the predicted loadbearing capacity when m varies (in this case $N = 40$). Similarly, when m is fixed, P_u depends on the number of blocks in which the semi-arch is divided (see Fig. 12c, with $m = 175$). Nevertheless, when $m \geq 50$ and $N \geq 20$, the mesh dependence vanishes, and the proposed model estimates a value of P_u (0.42 kN) close to that experimentally measured (0.44 kN). Obviously, the values of m and n are not the same for all arches and vaults, thus the limit analysis must be iteratively performed by increasing m and N until the numerical results do not change.

4.2. Masonry vaults under fire

In addition to the fire tests described in Section 3, also the barrel vault investigated by Vigili del Fuoco [28] (hereinafter called vault #3) is taken into consideration for the validation of the proposed model. Vault #3 had clean span length = 1610 mm, intrados radius = 930 mm (465 mm rise), and a cross-section of 2070 × 120 mm^2. Eight bricks of 55 × 120 × 250 mm^3 and premixed cement-lime based mortar were used for layering the vault (mean compressive strength f_m = 11.80 N/mm^2). In order to represent the backfill, two

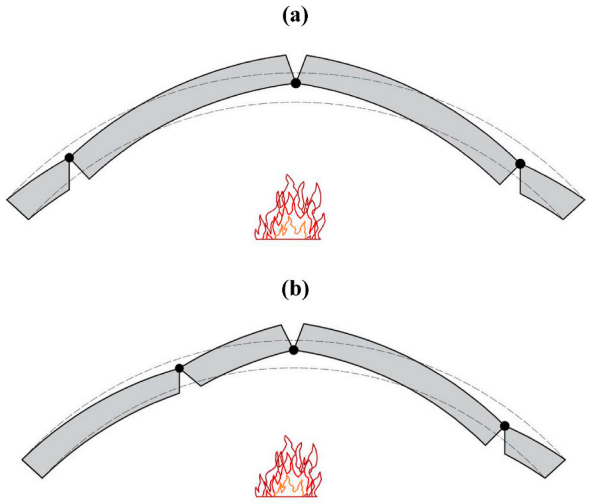

Fig. 11. Qualitative positions of hinges in (a) vault #1 and (b) vault #2.

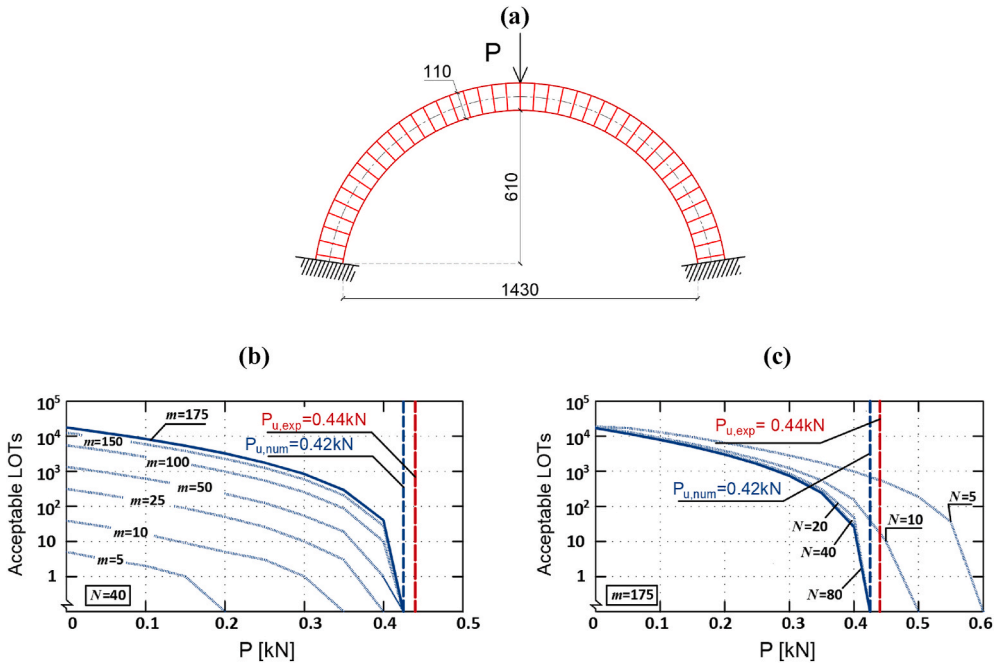

Fig. 12. Masonry arch in absence of fire: (a) Geometry of the arch [34] (measures in mm); (b) Numerical results as a function of the number of LOTs - *m*. (c) Numerical results as a function of the number of blocks – *N* [Number of LOT plotted in logarithmic scale].

concentrated loads (of 9.2 kN each) were symmetrically applied at 500 mm from the crown (see Fig. 13 and Table 4). The test was intentionally interrupted after 52 min, although neither collapses nor spalling occurred.

Fig. 14 illustrates the comparison between the numerical predictions of the fire resistance R (i.e., the maximum time at which the number of acceptable LOT remains greater than zero) and those experimentally measured in vault #1 (Fig. 14a), vault #2 (Fig. 14b) and vault #3 (Fig. 14c). In all the cases, numerical values of R are computed by assuming $N = 80$ and $m = 200$.

For vault #1, Fig. 14a shows the decrement in the number of the acceptable LOTs as the time of exposure to the standard fire increases. This is mainly due to the reduction of the resisting cross-sectional area of the vault during the first stage of fire exposure. Afterwards, the resulting stresses $\sigma_{Ed,i}$, along the LOTs, tend to be larger than the compressive strength f_d (Fig. 4).

According to the numerical results, vault #1 fails after 102 min of exposure. However, since the fire exposure lasted only 90 min, it is not possible to assess whether the estimated value of R is conservative or not.

A similar decrement of the acceptable LOTs also occurs in vault #2 and vault #3, as illustrated in Fig. 14b and c, respectively. Nevertheless, the duration of tests (115 min in vault #2 and 52 min in vault #3) was longer than the fire resistance estimated by the

Table 4
Summary of geometrical, mechanical and load properties taken from literature. (standard deviation and COV are reported within brackets; nd = "not declared").

Parameters		Masonry arch [35]	vault #3 [28]
Span	(mm)	1430	1611
Rise	(mm)	610	465
Thickness	(mm)	110	120
Width	(mm)	245	2070
Intrados radius (mm)	(mm)	720	930
Arch angle	(°)	164	120
Compressive strength[a]	(MPa)	19.5 (nd; nd)	11.80 (1.40; 0.119)
Self-weights	(kN/m^3)	16.00	17.00
Backfill	(kN/m^3)	0	0
Live loads	(kN/m^2)	0	0
Concentrated loads	(kN)	0.44 (at failure)	9.2 (two loads)

[a] Mean compressive strength measured in uniaxial compression on masonry prism with different sizes.

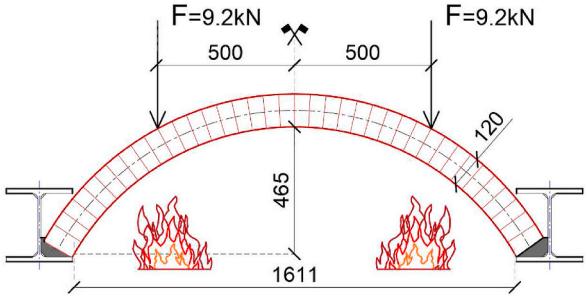

Fig. 13. Geometry and load arrangement of vault #3 [28] (measures in mm).

proposed model (i.e., R = 100 min for vault #2, and R = 28 min for vault #3). In other words, in vaults subjected to concentrated or uniformly distributed loads (in addition to self-weight) and to a standard fire in the intrados, the proposed model generally provides a conservative evaluation of the fire resistance.

5. Conclusions

As the fire resistance of curvilinear masonry structures has been scarcely investigated before, new theoretical and experimental investigations have been proposed. Based on the results of these analyses, the following conclusions can be drawn:

1. The failure of masonry barrel vaults occurs in presence of a four-hinge mechanism, even in the case of fire action. The hinges are the consequence of the brick-mortar interface failure.
2. When spalling does not occur, dead loads do not vary during the fire exposure, although the area of resisting cross-section reduces with the increment of temperature.
3. The fire resistance of masonry arches and vaults can be evaluated by combining the limit analyses, generally used for explicit loads, with the residual cross-section method, currently adopted in the simplified structural analysis of columns and walls.
4. Compared to some test results, with and without the exposure to fire, the proposed model seems to provide a conservative evaluation of the load bearing capacity of arches and vaults.

The proposed model can be used to assess arches and vaults having a symmetry (not only for the geometry, but also for material properties and load arrangement) with respect to the keystone cross-section. In asymmetrical cases, more refined models have to be introduced to analyse the fire resistance. Thus, future research will be devoted to the introduction of an advanced numerical model, in accordance with the Annex D of Eurocode 6 – Part 1–2 [16]. By means of this model, a sensitivity analyses can also be performed on arches and vaults of different sizes and shapes, with the aim of identifying the most impactful parameters.

Authors contribution

"Conceptualization, A.P.F. and N.S.B.; Methodology, A.P.F. and N.S.B.; Software, N.S.B.; Validation, A.P.F. and N.S.B.; Investigation, A.P.F. and N.S.B.; Data Curation, A.P.F. and N.S.B.; Writing – Original Draft Preparation, A.P.F. and N.S.B.; Writing – Review & Editing, A.P.F. and N.S.B.; Project Administration and Funding Acquisition, A.P.F.

Declaration of competing interest

The authors declare that they have no known competing financial interests or personal relationships that could have appeared to influence the work reported in this paper.

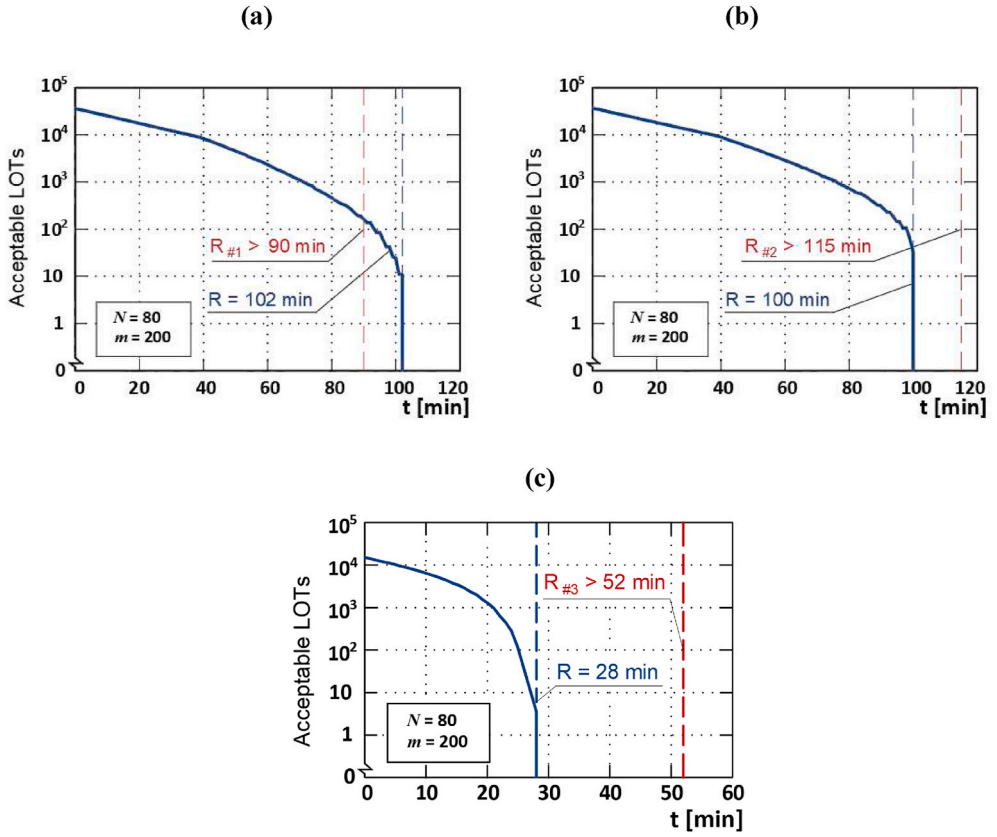

Fig. 14. Comparison between experimental and numerical results of (a) vault #1, (b) vault #2, and (c) vault #3. [Number of LOT plotted in a logarithmic scale].

Acknowledgements

The authors wish to thank San Paolo Foundation for financing the experimental campaign.

References

[1] at al C. Melbourne, J. Wang, A. Tomor, G. Holm, M. Smith, P.E. Bengtsson, J. Bien, T. Kaminski, P. Rawa, J.R. Casas, P. Roca, C. Molins, Sustainable Bridges – Assessment for Future Traffic Demands and Longer Lives, 2007. Deliverable D4.7, SB-4.7.
[2] G. De Matteis, D. Cacace, J. Rouhi, Masonry Vaults: Architectural Evolution, Structural Behaviour and Collapse Mechanisms, 2019. Proceedings of the 7th Structural Engineers World Congress.
[3] A.M. D'Altri, V. Sarhosis, G. Milani, J. Rots, S. Cattari, S. Lagomarsino5, E. Sacco, A. Tralli, G. Castellazzi, S. de Miranda, Modeling strategies for the computational analysis of unreinforced masonry structures: Review and classification, Arch. Comput. Methods Eng. 27 (2020) 1153–1185, https://doi.org/10.1007/s11831-019-09351-x.
[4] M. Cerone, G. Croci, A. Viskovic, The Structural Behaviour of Colosseum over the Centuries, More than Two Thousand Years in the History of Architecture, 2000 (online at colosseum-over-centuries-1f.PDF (the-colosseum.net)).
[5] J. Heyman, The Stone Skeleton: Structural Engineering of Masonry Architecture, Cambridge University Press, 1997.
[6] P.B. Lourenco, Computations on historic masonry structures, Prog. Struct. Eng. Mater. 4 (2002) 301–319, https://doi.org/10.1002/pse.120.
[7] UNI EN 1996-1-1, Eurocode 6 - Design of Masonry Structures - Part 1-1: General Rules for Reinforced and Unreinforced Masonry Structures, 2005.
[8] R. Barsotti, S. Bennati, A simple and effective nonlinear elastic one-dimensional model for the structural analysis of masonry arches, Meccanica 53 (2018) 1899–1915, https://doi.org/10.1007/s11012-017-0711-4.
[9] A. Audenaert, P. Fanningb, L. Sobczakb, H. Peremansa, 2-D analysis of arch bridges using an elasto-plastic material model, Eng. Struct. 30 (2008) 845–855.
[10] C. Scuro, F. Lamonaca, R. Codispoti, D. Carnì, R.S. Olivito, Experimental and numerical analysis on masonry arch built with fictile tubules bricks, Measurement 130 (2018) 246–254.
[11] D. Ferretti, C. Boni, E. Lenticchia, Effects of brick pattern on the static behavior of masonry vaults, Int. J. Architect. Herit. (2021), https://doi.org/10.1080/15583058.2021.1874565.
[12] ISO 834-1:1999: Fire-Resistance Tests - Elements of Building Construction — Part 1: General Requirements.
[13] S.J. Lawrence, N. Gnanakrishnan, The Fire Resistance of Masonry Walls - an Overview, 1987, pp. 431–437. Fire National Structural Engineering Conference, Melbourne, 26–28 August.
[14] S.M. Byrne, Fire resistance of load-bearing masonry walls, Fire Technol. 15 (1979) 180–188.
[15] N. Gnanakrishnan, The Effect of End Restraint on the Stability of Masonry Walls Exposed to Fire, National Building Technology Centre, Technical Records No. 531Technology Centre.
[16] UNI EN 1996-1-2 2005: Eurocode 6 - Design of Masonry Structures - Part 1-2: General Rules - Structural Fire Design.
[17] M. Andreini, M. Sassu, Mechanical behaviour of full unit masonry panels under fire action, Fire Saf. J. 46 (2011) 440–450.
[18] A. Nadjai, D. Laverty, M. O'Garra, Behaviour of compartment masonry walls in fire situation, Fire Mater. 27 (2003) 163–182, https://doi.org/10.1002/fam.824.
[19] T. Nguyen, F. Meftah, R. Chammas, A. Mebarki, The behaviour of masonry walls subjected to fire : modelling and parametrical studies in the case of hollow burnt-clay bricks, Fire Saf. J. 44 (2009) 629–641.

[20] E. Donval, D. Pham, G. Hassen, P. de Buhan, D. Pallix, Determination of the deformed shape of a masonry wall exposed to fire loading by a homogenization method, IOP Conf. Ser. Mater. Sci. Eng. 1203 (2021), https://doi.org/10.1088/1757-899X/1203/3/032076.
[21] M. Andreini, A. de Falco, M. Sassu, Stress–strain curves for masonry materials exposed to fire action, Fire Saf. J. 69 (2014) 43–56.
[22] J. Brulin, E. Blond, E. de Bilbao, A. Rekik, M. Landreau, A. Gasser, Y. Colleville, Methodology for brick/mortar interface strength characterization at high temperature, Construct. Build. Mater. 265 (2020), 120565.
[23] A. Daware, M.Z. Naser, Fire performance of masonry under various testing methods, Construct. Build. Mater. 289 (2021), 123183.
[24] J.J. Brooks, Concrete and Masonry Movements, first ed., 2015, https://doi.org/10.1016/C2013-0-19554-2.
[25] S. Russo, F. Sciarretta, Masonry exposed to high temperatures: mechanical behaviour and properties—an overview, Fire Saf. J. 55 (2013) 69–86, https://doi.org/10.1016/j.firesaf.2012.10.001.
[26] S. Masse, G. Vetter, F. Boch, C. Haehnel, Elastic modulus changes in cementitious materials submitted to thermal treatments up to 1000 °C, Adv. Cement Res. 14 (2002) 169–177.
[27] A. Fantilli, B. Chiaia, Modelling Masonry Arches under Fire, 2014, 9th International Masonry Conference, Guimarães.
[28] Vigili del Fuoco – DCPSP, Experimental fire test on a barrel vault (in Italian), http://www.vigilfuoco.it/aspx/download_file.aspx?id=19616, 2015.
[29] M. Gilbert, Limit Analysis Applied to Masonry Arch Bridges: State-Of-The-Art and Recent Developments, 5th International arch bridges conference, 2007. hms.civil.uminho.pt.
[30] W.J. Harvey, Stability, strength, elasticity and thrust lines in masonry structures, Struct. Eng. 69 (2001) 181–184.
[31] O.C. Zienkiewicz, R.L. Taylor, The Finite Element Method for Solid and Structure. Mechanics, sixth ed., Elsevier, Amsterdam, 2005.
[32] V. Alecci, F. Focacci, L. Rovero, G. Stipo, M. De Stefano, Extrados strengthening of brick masonry arches with PBO–FRCM composites: experimental and analytical investigations, Compos. Struct. 149 (2016) 184–196.
[33] D.V. Oliveira, I. Basilio, P.B. Lourenço, Experimental behavior of FRP strengthened masonry arches, J. Compos. Construct. 14 (2010), https://doi.org/10.1061/(ASCE)CC.1943-5614.0000086.
[34] V. Alecci, F. Focacci, L. Rovero, G. Stipo, M. De Stefano, Intrados strengthening of brick masonry arches with different FRCMcomposites: experimental and analytical investigations, Compos. Struct. 176 (2017) 898–909.
[35] P. Zampieri, N. Simoncello, J. Libreros, C. Pellegrino, Evaluation of the vertical load capacity of masonry arch bridges strengthened with FRCM or SFRM by limit analysis, Eng. Struct. 225 (2020), 111135.
[36] I. Cancelliere, M. Imbimbo, E. Sacco, Experimental tests and numerical modelling of reinforced masonry arches, Eng. Struct. 32 (2010) 776–792.

List of abbreviations and symbols

Abbreviations

LOT: Line of thrust

Symbols

b_1: width of the masonry cross-section
b_2: width of the backfill material
b_3: width of the surface where live loads are distributed
COV: coefficient of variation
$d_{PG1,i}$: distance of the force $P_{G1,i}$ from the I^{th}-1 cross-section
$d_{PG2,i}$: distance of the force $P_{G2,i}$ from the I^{th}-1 cross-section
$d_{PQv,i}$: distance of the force $P_{Qv,i}$ from the I^{th}-1 cross-section
$e_{k,w}$: eccentricity of the $S_{k,w}$
$f_{b,k}$: characteristic compressive strength of the bricks
f_k: characteristic compressive strength of the masonry unit
f_m: average value of compressive strength of a masonry unit
$f_{d\vartheta 1} = f_{d20}$: design compressive strength at $T = 20°$
$f_{d\vartheta 2} = 0$: design compressive strength of the fully damaged zone
$H_{b,I}$: depth of the I^{th} cross-section
H_k: intensity of the horizontal force in the keystone (kth LOT)
i: subscript used to numerate the blocks ($i = 1, 2, \ldots, N$)
I: subscript used to numerate the cross-sections ($I = 0, 1, 2, \ldots, n$)
j: subscript used to numerate the points of passage of the LOT_s ($I = 0$ and $I \frown N$)
k: subscript used to numerate the lines of thrust ($k = 1, 2, \ldots, m \times m$)
m: number of points of passage within springer and crown cross-section
$n = N + 1$: number of cross-sections in which the structure is divided
N: number of blocks in which the structure is divided
$P_{G1,i}$: load due to the self-weight of the ith block of masonry
$P_{G2,i}$: load due to the backfill material (sand or concrete) in the ith block
$P_{Qv,i}$: load due to Q_v in the ith block
P_I: concentrated load in the I^{th} cross-section
Q_v: live load
$R(i)$: resultant of applied loads in the ith block
R_{TOT}: resultant of the vertical loads in the structure
s.d.: standard deviation
s_{ineff}: ineffective thickness of the cross section
S_k: reaction in the support (kth LOT)
$S_{k,w}$: inclined resultant acting in the wth cross-section (kth LOT)
t: time
T: temperature
w: subscript used to numerate the points of the kth LOT ($w = 0, 1, 2, \ldots, N+1$))
y_{kO}: ordinate of the wth point (kth LOT)
$y_{sup,I}$: ordinate of the upper edge of the backfill material in the I^{th} cross-section
z_I: abscissa of the I^{th} cross-section
z_{kO}: abscissa of the wth point (kth LOT)
$z_R(i)$: abscissa of the resultant R(i)
z_{Rtot}: abscissa of R_{Tot}
α_i: angle of inclination of the ith block

β_k: angle of inclination of S_k (kth LOT)
$\alpha_{k,w}$: angle of inclination of the wth $S_{k,w}$
$\Delta z_i = z_I - z_{I-1}$: length of the ith block
γ_{G1}: density of the masonry material
γ_{G2}: density of backfill material
γ_c: density of concrete
γ_s: density of loose sand
θ_1: maximum temperature at which $f_{d\,\theta 1} = f_{d20}$
θ_2: temperature at which $f_{d\theta\,2} = 0$
$\sigma_{Ed,w}$: compressive stress in the wth cross-section (kth LOT)